

Correlations in STAR: interferometry and event structure

Mikhail Kopytine for the STAR Collaboration

Department of Physics, Kent State University, Kent, Ohio, USA

E-mail: kopytin@bnl.gov

Abstract. STAR observes a complex picture of RHIC collisions where correlation effects of different origins – initial state geometry, semi-hard scattering, hadronization, as well as final state interactions such as quantum intensity interference – coexist. Presenting the measurements of flow, mini-jet deformation, modified hadronization, and the Hanbury Brown and Twiss effect, we trace the history of the system from the initial to the final state. The resulting picture is discussed in the context of identifying the relevant degrees of freedom and the likely equilibration mechanism.

1. Introduction

This talk is an overview of recent STAR results in the field known as "correlations and fluctuations". Out of multiple reasons to analyze correlations and fluctuations at RHIC known before the data became available, there is one that seems to dominate now: by measuring correlations and their evolution we learn about *equilibration* of the system. Is it taking place? What is the mechanism? And what is equilibrating? Novel and advanced data analysis techniques have been created lately to address these issues. I will focus on the developments since Quark Matter 2004.

Our evidence for equilibration includes elliptic flow, medium modification of mini-jets and of charge-dependent correlations. Related issues are the azimuthally-sensitive HBT and the blast wave picture.

2. Elliptic and directed flow as a particle number correlation

In non-central collisions the initial spatial configuration is anisotropic. But the configuration space anisotropy does not produce momentum space anisotropy unless there is another mechanism involved, such as local equilibration via rescattering. If the latter is occurring, then it is sensible to talk about pressure gradients, and the azimuthal variation thereof. This picture naturally calls for analysis of correlations in velocity between local elements of expanding matter, but experimentally one is limited to final state particles. The flow analysis in this field began with diagonalization of the (*momenta*-based) sphericity tensor [1]. In experiments with limited acceptance in rapidity at higher energies (AGS, SPS and RHIC) a different technique [2] became popular which utilizes the observed azimuthal anisotropy by expanding the particle *number*

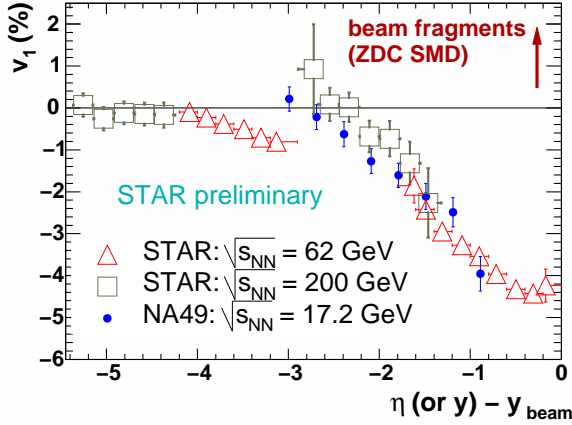


Figure 1. Directed flow coefficient as a function of pseudorapidity relative to the projectile beam in STAR and NA49

distribution with respect to the reaction plane angle Ψ_r into a Fourier series

$$E \frac{d^3 N}{d^3 p} = \frac{1}{2\pi} \frac{d^2 N}{p_t dp_t dy} \left\{ 1 + \sum_{m=1}^{\infty} 2v_m \cos[m(\phi - \Psi_r)] \right\}, \quad (1)$$

with v_2 typically being the largest component. Cumulant-based analyses, developed later [3], distinguish between two-particle and higher order correlations and separate flow (a multiparticle correlation) from the lower-order "non-flow".

STAR's recent measurements of directed flow (v_1), shown in Fig.1, use 3-particle cumulants to minimize the "non-flow" effects. In the limiting fragmentation picture [4], what matters for the fragmenting system is the relative rapidity with the nearby spectators, hence the choice of the abscissa. The data from different energies are consistent with limiting fragmentation. The v_1 term requires knowledge of Ψ_r between 0 and 2π and thus an azimuthal direction rather than orientation of the reaction plane. This direction, given by the spectators, is reconstructed event-by-event by means of a position-sensitive zero-degree shower-maximum detector (ZDC SMD) which selectively detects fragmentation neutrons behind a RHIC dipole magnet. These measurements indicate that the directed flow at RHIC is opposite in azimuthal angle to the direction of the spectators (an "anti-flow"). We will return to the velocity aspect of the elliptic flow in Sections 3 and 6.

3. Final state geometry

While v_m characterize the particle distribution in momentum space, observation of the corresponding structure in the configuration space rests with the Hanbury Brown-Twiss (HBT) interferometry. Herein a correlation function is defined as the ratio of two-particle probability density to the uncorrelated reference, which in STAR is obtained by forming mixed pairs. In the Cartesian parameterization,

$$C_{\text{fit}}(\vec{q}) = 1 + \lambda \exp(-q_o^2 R_o^2 - q_s^2 R_s^2 - q_l^2 R_l^2), \quad (2)$$

the momenta of a pair are projected onto the transverse plane where one identifies directions of their sum and difference. Projections of the momentum difference on those directions become, respectively, outward q_o and sideward q_s components. The longitudinal component q_l is orthogonal to both of them. Corresponding to q are the radii parameters R . Fig.2 shows a $\sqrt{s_{NN}}$ dependence of the quantities representing the best fits of the parameters in Eq.2 to the experimental data. The bottom panel presents density of π^+ multiplicity per unit of rapidity, which displays a steady logarithmic increase with $\sqrt{s_{NN}}$. The latter may be contrasted with

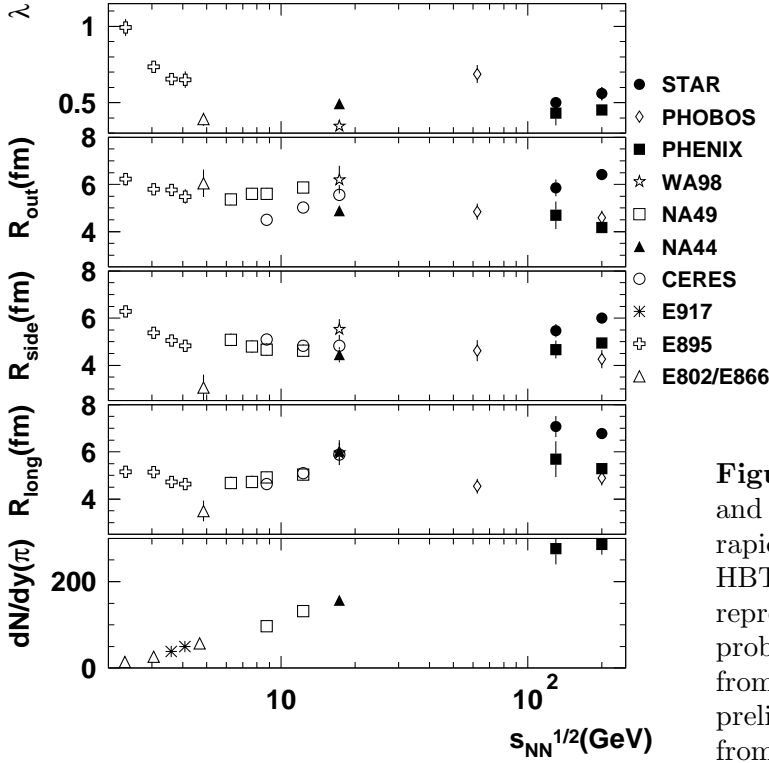


Figure 2. Fit parameters for $\pi^-\pi^-$ and dN/dy of π^+ at or near mid-rapidity as a function of $\sqrt{s_{NN}}$. The HBT data are either p_t integrals or represent a p_t bin closest to the most probable inclusive p_t and are taken from [7]. The NA49 HBT data are preliminary. The dN/dy data are from [8].

the general lack of energy dependence of the radius parameters which underscores the non-triviality of interpreting the HBT results. In the hydrodynamical framework the concept of *length of homogeneity*¹ has been introduced [5], and it is known that the measured radii reflect those lengths² (or rather, according to [6], a combined effect of the correlation lengths in the *primordial correlator* between the *currents* emitting the pion radiation and the source size). These lengths are smaller than the geometrical source sizes in an expanding (due to pressure gradients) and thus inhomogeneous system. A more subtle issue is that of the little relative difference between R_o and R_s , which is believed to increase with longer emission.

The quantitative understanding of this information remains a model-dependent problem. In particular, one may assume a local, thermally-equilibrated system and thus ascribe all the sources of inhomogeneity (dynamical correlations) to hydrodynamic expansion. Taking this approach and fitting the data (including single-particle spectra) with the modified Blast Wave model, Retiere and Lisa obtained a set of parameters [10]. Remarkably, the azimuthally-varying component ρ_2 in their description of the transverse velocity field appears to be non-zero and well constrained by the fit. This represents an indirect measurement of the transverse-velocity aspect of elliptic flow which complements the particle-number-related v_2 .

The azimuthally-dependent radii recently published by STAR [9] show an effective source elongated perpendicularly to the reaction plane. This indicates shorter homogeneity lengths (and thus larger gradients) in-plane than out-of-plane, which is consistent with the geometry of the early stage of the collision. The early emission is consistent with short emission time.

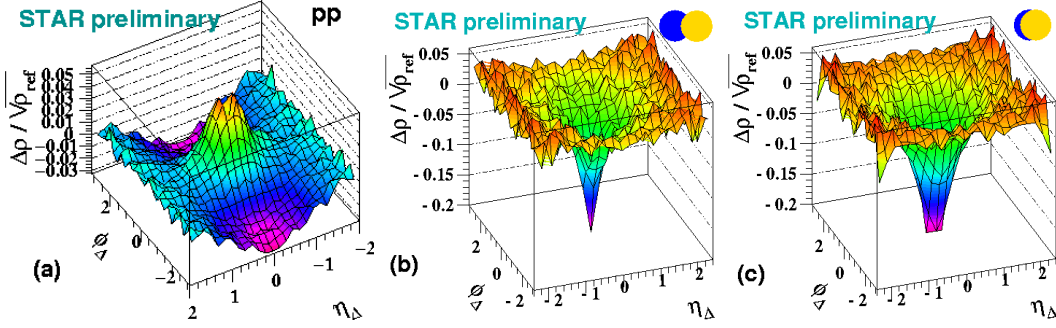


Figure 3. Comparison of CD correlations in η and ϕ : (a) pp collisions at $\sqrt{s} = 200$ GeV, (b) peripheral AuAu collisions, (c) central AuAu collisions. (b) and (c) are at $\sqrt{s_{NN}} = 130$ GeV.

4. Charge-dependent number correlations– modified hadronization in the medium

The charge-dependent (CD) number correlation is defined as a difference between the like-sign and the unlike-sign correlations. (In this and subsequent sections we discuss results obtained without particle identification). The correlations are defined by comparing same-event pairs with mixed-event pairs, obtained from mixing similar events. To characterize and normalize correlations, we use

$$\frac{\Delta\rho}{\sqrt{\rho_{\text{ref}}}} = \frac{\rho_{a,b} - \rho_a\rho_b}{\sqrt{\rho_a\rho_b}}, \quad (3)$$

where a and b index particles (or in the discretized case, bins in the kinematic space occupied by particles), $\rho_{a,b}$ is pair density distribution, while ρ_a and ρ_b are the corresponding single-particle distributions, whose product forms the reference density ρ_{ref} . Experimentally one deals with fluctuating histogram bin contents n_a and n_b and Eq.3 becomes (see Appendix A)

$$\frac{\Delta\rho}{\sqrt{\rho_{\text{ref}}}} \rightarrow \frac{\overline{n_a n_b} - \overline{n_a} \times \overline{n_b}}{\sqrt{\overline{n_a} \times \overline{n_b}}} = \frac{\text{Cov}[n_a, n_b]}{\sqrt{\overline{n_a} \times \overline{n_b}}} \quad (4)$$

If the variance in the bin population n is dominated by the Poissonian process, $\text{Var}[n] = \overline{n}$, and if in presence of correlations $\text{Cov}[n_a, n_b] \propto \text{Var}[n]$ (number of correlation sources is proportional to multiplicity) this normalization eliminates the trivial multiplicity dependence of the correlation amplitude. Eq.3 represents a *per-particle* measure of correlations.³

In paper [15], CD correlations in η and ϕ have been analyzed simultaneously by using *joint autocorrelation*. Fig.3 shows a comparison of CD correlations in pp collisions (panel (a)) with peripheral and central AuAu collisions. Kinematic cuts on the track separation are applied to eliminate the contribution of HBT and Coulomb effects in AuAu collisions (panels (b) and (c)) [15]. A much broader HBT correlation for pp collisions contributes the gaussian peak at the origin in (a). Transverse momentum conservation also contributes to the structure at the origin (the ridge beneath the gaussian peak). The main feature, the negative gaussian peak on η_{Δ} , is attributed to local charge conservation during hadronization. If the process happens on a longitudinally expanding string (as e.g. in Lund model), the strict alternation of positive and negative hadrons in rapidity holds (modulo interspersed neutrals). This implies that η_{Δ} for an unlike-sign pair tends to be shorter than for the like sign, regardless of ϕ_{Δ} , creating a groove in the CD plot, clearly seen in Fig.3(a). The ϕ_{Δ} -independent groove appears to diminish in

¹ The term “effective length” was used in the original article.

² This result was derived for locally thermally equilibrated systems.

³ In this terminology, the correlation function commonly used in HBT represents a *per-particle-pair-normalized* quantity. The choice of normalization depends on the correlation mechanism under study.

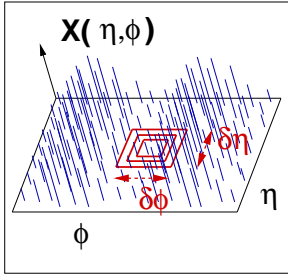


Figure 4. A fantasy event. Positions of spikes indicate η, ϕ kinematics of individual particles, their heights – magnitude of quantity X assigned to a particle, which could be p_t or a derived quantity. This event has azimuthal anisotropy, however its v_2 may be 0, illustrating the difference between number and p_t flow. The analysis proceeds by selecting a bin of size $\delta\eta, \delta\phi$, integrating the *random field* X within the bin, finding the variance of that integral in an event sample, then feeding this information into an integral equation to yield the correlation of X , as discussed in Appendix B.

amplitude from (a) and (b) to (c). In addition, the negative peak at 0 relative angle changes its shape, becoming narrower from peripheral to central AuAu collisions and acquiring more η - ϕ symmetry. We hypothesize that this reflects a change in the hadronization geometry from one dominated by independent string break-ups in peripheral collisions to a bulk hadronization process in which individual strings are no longer relevant.

5. Charge-independent number correlations – longitudinal minijet deformation

The charge-independent (CI) number correlation sums the like-sign and the unlike-sign correlations. In AuAu collisions, these correlations have been analyzed by STAR in the space of pseudorapidity η and azimuthal angle ϕ [11, 13] and in the transverse momentum space [12].

Our discrete-wavelet technique [11] extracts information about correlation structure by measuring the power spectra of local fluctuations in the density of charged hadrons with respect to a mixed-event reference (the so-called “dynamic texture” of the event). As discussed in [14], this observable is a measure of the gradient of the two-particle correlation function, but takes less computing.⁴

The experiment [11] reveals a reduction in the dynamic texture (and thus in the correlation function gradient) along the η -direction at $p_t > 0.6$ GeV/c in the central AuAu collisions, compared to an expectation based on peripheral events. HIJING simulations [11] point to minijets as the likely source of correlations of this scale and magnitude. The possible mechanism of the reduction is a coupling between the minijet fragments and the longitudinally expanding bulk medium. In paper [13], the same correlation structure is investigated in the joint η - ϕ autocorrelation technique. It is found that the correlations are broadened in η_Δ with centrality. A reduction in the correlation gradient (“dynamic texture”) and the elongation of the correlation function along η_Δ are consistent descriptions of the effect.

6. p_t correlations –minijets and elliptic flow

We require a direct measurement of correlations in the velocity field, independent of particle number correlations. To form an independent measurement, these have to be separated from particle number correlations. For a random field (such as particle number or velocity distributed in η and ϕ , see Fig.4) variance of the integrated content of a bin can be related via an integral equation to the correlation function of the field [16, 17]. The correlation function can be reconstructed from the measured variance by solving the integral equation derived in [16, 17]. This process offers a computational advantage since the bin integration involves $\mathcal{O}(N)$ computations, whereas two-particle correlations require $\mathcal{O}(N^2)$ (N is the event multiplicity used). By varying the bin size one varies the range of the difference variable in the correlation function.

⁴ The number of computations required is $\mathcal{O}(N)$, in contrast with $\mathcal{O}(N^2)$ required for direct construction of the correlation function.

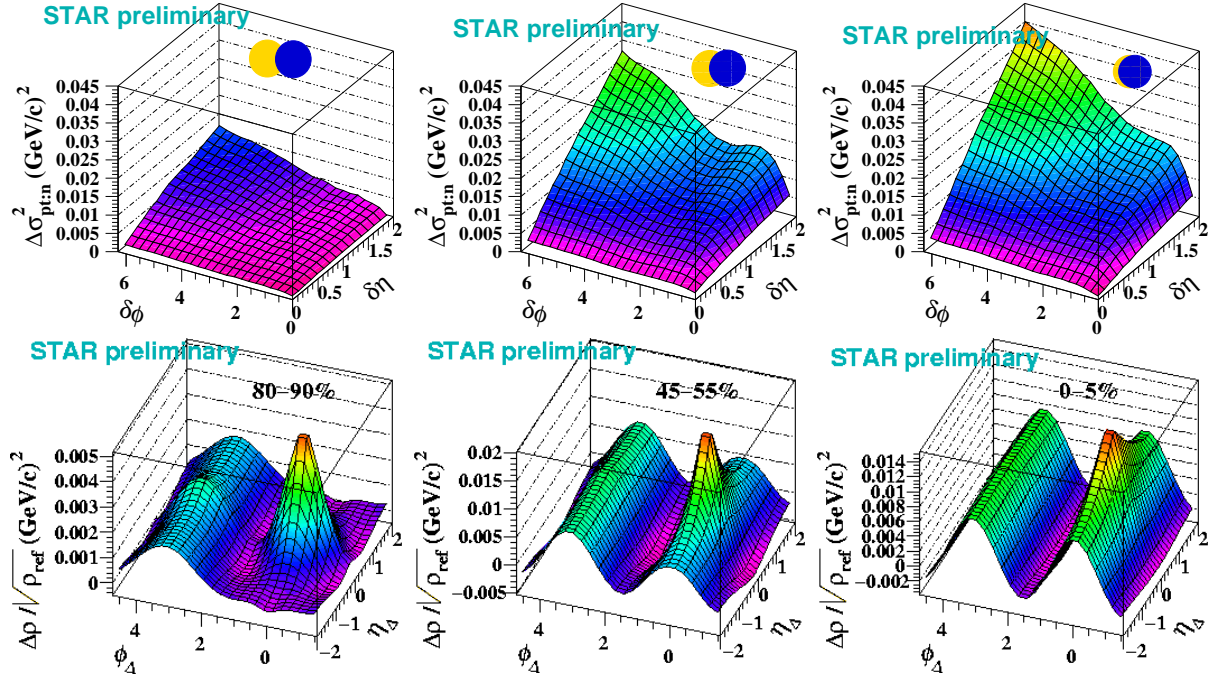


Figure 5. Top: scale dependence of the reference-subtracted variance $\Delta\sigma_{pt:n}^2$. Bottom: reference-subtracted normalized correlation functions reconstructed from $\Delta\sigma_{pt:n}^2$ by inversion. The percentage intervals indicate centrality for each column-wise pair of plots.

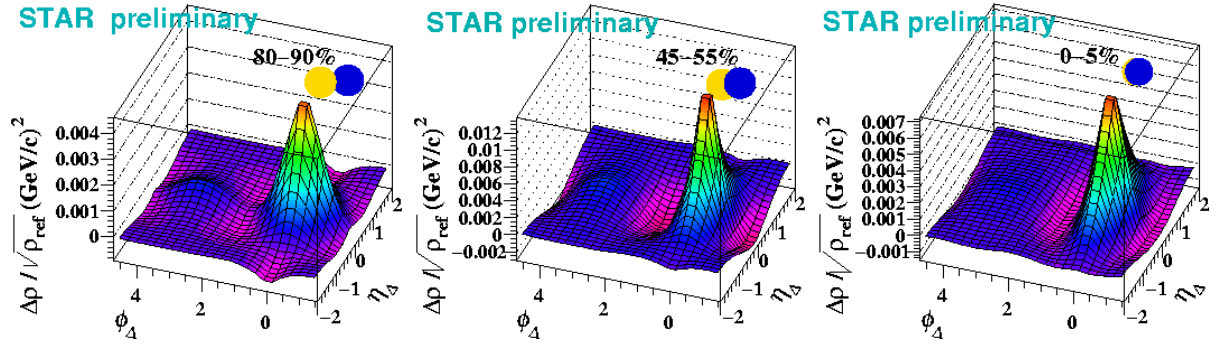


Figure 6. Same data as in Fig.5 with subtracted azimuthal harmonics v_1 and v_2 .

In order to extract the p_t correlation alone, we need to disentangle the effect of n from that of $p_{t,i}$ in the variance of $p_t \equiv \sum_{i \in (\eta, \phi) \text{ bin}} p_{t,i}$, and from statistical fluctuations. We denote the desired variance as $\Delta\sigma_{p_t:n}^2$. As an estimator of $\Delta\sigma_{p_t:n}^2$, we use $\text{Var}[p_t - n\hat{p}_t]/\bar{n} - \sigma_{p_t}^2$, where the latter term is the inclusive per-hadron p_t variance. In the case when p_t in the bin, event-by-event, derives from the same parent distribution (not the case in Fig.4), $\Delta\sigma_{p_t:n}^2$ converges to 0, despite fluctuations (statistical or not) in n .

Top panels in Fig.5 represent scale dependence of the variance $\Delta\sigma_{p_t:n}^2$ for three centrality classes. The bottom panels, representing per-particle normalized correlations plotted on difference variables, are obtained from the respective top panels by solving the integral equation derived in [16, 17] (see Appendix B) which relates variance and correlation.

While the quadrupole wave in Fig.5(bottom row) is the reflection of the elliptic flow in the $p_t : n$ correlation function, the peak at 0 angle differences likely reflects minijets [19]. But unlike

flow, the effect of minijets on the HBT radii at RHIC energy is not part of the standard (local equilibrium) picture. Therefore this effect may constitute an under-appreciated factor driving the effective radii (Fig.2) down at higher $\sqrt{s_{NN}}$.

The amplitude of the minijet peak has a non-monotonic behavior with increasing centrality, rising in peripheral and falling in central collisions. The peak is seen to be elongated longitudinally in central collisions, showing qualitatively the same behavior as seen with number correlations by using wavelet analysis and joint autocorrelation (Section5).

7. Conclusions

The small effective HBT radii at RHIC indicate that the system is highly inhomogeneous and decouples rapidly. STAR has evidence that semi-hard scattering leaves a trace in the "soft" p_t domain which is usually considered a safe realm for local equilibrium approximations, thus possibly explaining some of the inhomogeneity. Whether or not the minijet correlations present a challenge to the picture of local equilibrium which constitutes a basis for much of the HBT interpretation infrastructure, will depend on the effective final-state-particle number involved in a minijet, or in other words, on the *order* of those correlations (higher order being more hydro-like and thus probably less of a challenge). Therefore a study of higher order correlations and cumulants may be a promising future direction. The phenomenon of η -broadening of minijets at "soft" p_t (Section 5 and 6) can clarify the nature of the medium created in central AuAu collisions, provided that the coupling mechanism, apparently sensitive to that nature, is under theoretical control.

Appendix A. Notation

In our notation i is particle index, n is number of particles within a kinematic cut (bin), $\overline{(\dots)}$ denotes an average over events, \hat{p}_t is an inclusive mean p_t per particle, x_Δ (variants: η_Δ , ϕ_Δ) is difference variable = $x_i - x_{i'}$, δx is scale (range of local integration, see Fig.4), Δx is the upper limit on δx . Covariance of x and y is denoted as $\text{Cov}[x, y]$, variance of x – as $\text{Var}[x]$.

Appendix B. From variance to correlation

The connection between variance and correlation function – the basis of analysis in Section6 – is discussed in detail using integral calculus in [16] and the algebra of discrete bins in [17]. For a random field $X(t)$, the *autocorrelation* function is defined [18] as

$$\rho(X, t_\Delta) \equiv \overline{X(t)X(t+t_\Delta)} \quad (\text{B.1})$$

(assuming that correlations do not depend on position t).

The variance of X , integrated over bin of width $\delta\eta, \delta\phi$, centered at 0 (see Fig.4) is

$$\text{Var}[X; \delta\eta, \delta\phi] = \overline{\left(\int_{-\delta\eta/2}^{\delta\eta/2} \int_{-\delta\phi/2}^{\delta\phi/2} X d\eta d\phi \right)^2} - \left(\int_{-\delta\eta/2}^{\delta\eta/2} \int_{-\delta\phi/2}^{\delta\phi/2} \overline{X} d\eta d\phi \right)^2 = \quad (\text{B.2})$$

$$\int_{-\delta\eta/2}^{\delta\eta/2} d\eta_1 \int_{-\delta\phi/2}^{\delta\phi/2} d\phi_1 \int_{-\delta\eta/2}^{\delta\eta/2} d\eta_2 \int_{-\delta\phi/2}^{\delta\phi/2} d\phi_2 [\overline{X(\eta_1, \phi_1)X(\eta_2, \phi_2)} - \overline{X(\eta_1, \phi_1)} \times \overline{X(\eta_2, \phi_2)}] \quad (\text{B.3})$$

As we form the reference-subtracted variance $\Delta\sigma_X^2 \equiv \text{Var}[X; \delta\eta, \delta\phi] - \text{Var}[X_{\text{ref}}; \delta\eta, \delta\phi]$, the first term in the brackets above becomes the reference-subtracted correlation $\Delta\rho(X, \eta_\Delta, \phi_\Delta)$ and the second term cancels with the reference since $\overline{X} = \overline{X_{\text{ref}}}$.

$$\Delta\sigma_X^2 = \int_{-\delta\eta/2}^{\delta\eta/2} d\eta_1 \int_{-\delta\phi/2}^{\delta\phi/2} d\phi_1 \int_{-\delta\eta/2}^{\delta\eta/2} d\eta_2 \int_{-\delta\phi/2}^{\delta\phi/2} d\phi_2 \Delta\rho(X, \eta_1 - \eta_2, \phi_1 - \phi_2) \quad (\text{B.4})$$

$$= 2 \int_0^{\delta\eta} d\eta_\Delta \int_0^{\delta\phi} d\phi_\Delta (\delta\eta - \eta_\Delta)(\delta\phi - \phi_\Delta) \Delta\rho(X, \eta_\Delta, \phi_\Delta) \quad (\text{B.5})$$

Eq.B.5 is obtained by making a change of the integration variables from η_1, η_2 to η_1 and $\eta_\Delta = \eta_1 - \eta_2$, integrating over η_1 , and repeating the same for ϕ (see [16] for details). In the actual analysis, this integral equation is discretized by partitioning the acceptance into $m_\delta \times n_\delta$ *microbins* of size $\varepsilon_\eta \times \varepsilon_\phi$. X is replaced by $(p_t - n\hat{p}_t)/\sqrt{n}$. This denominator creates the reference number correlation $\rho_{\text{ref}}(n)$ in the final expression B.6 which makes it a per-particle measure:

$$\Delta\sigma_{p_t:n}^2(m_\delta\varepsilon_\eta, n_\delta\varepsilon_\phi) = 4 \sum_{k,l=1}^{m_\delta, n_\delta} \varepsilon_\eta\varepsilon_\phi K_{m_\delta n_\delta:kl} \frac{\Delta\rho(p_t : n; k\varepsilon_\eta, l\varepsilon_\phi)}{\sqrt{\rho_{\text{ref}}(n; k\varepsilon_\eta, l\varepsilon_\phi)}} \quad (\text{B.6})$$

Here the kernel K is a discrete representation of the continuous case :

$$(\delta\eta - \eta_\Delta)(\delta\phi - \phi_\Delta) \rightarrow \varepsilon_\eta\varepsilon_\phi K_{m_\delta n_\delta:kl} \equiv \varepsilon_\eta\varepsilon_\phi (m_\delta - k + \frac{1}{2})(n_\delta - l + \frac{1}{2}) \quad (\text{B.7})$$

Knowing the computationally cheaper quantity $\Delta\sigma_{p_t:n}^2$, we solve the integral equation B.6 for $\Delta\rho/\sqrt{\rho_{\text{ref}}}$ using standard numerical techniques [17].

References

- [1] Gutbrod H H, Poskanzer A M and Ritter H G 1989 *Rept. Prog. Phys.* **52** 1267
- [2] Voloshin S A and Zhang Y 1996 *Z. Phys. C* **70** 665
Poskanzer A M and Voloshin S A 1998 *Phys. Rev. C* **58** 1671
- [3] STAR Collaboration 2002 *Phys. Rev. C* **66** 034904
- [4] Benecke J, Chou T T, Yang C N and Yen E 1969 *Phys. Rev.* **188** 2159
- [5] Makhlin A N and Sinyukov Yu M 1988 *Z. Phys. C* **39**
- [6] Weiner R 2000 *Bose-Einstein Correlations and Subatomic Interferometry* (New York:Wiley)
- [7] PHOBOS Collaboration 2004 *Preprint* nucl-ex/0409001,
STAR Collaboration 2004 *Preprint* nucl-ex/0411036,
PHENIX Collaboration 2002 *Phys. Rev. Lett.* **88** 192302
PHENIX Collaboration 2004 *Phys. Rev. Lett.* **93** 152302
E895 Collaboration 2000 *Phys. Rev. Lett.* **84** 2798,
NA44 Collaboration 1998 *Phys. Rev. C* **58** 1656,
Kniege S for the NA49 Collaboration 2004 *J. Phys. G* **30** S1073,
E802 Collaboration 2002 *Phys. Rev. C* **66** 054906,
CERES Collaboration 2002 *Nucl. Phys. A* **714** 124,
WA98 Collaboration 2000 *Eur. Phys. J. C* **16** 445,
- [8] PHENIX Collaboration 2004 *Phys. Rev. C* **69** 024904,
PHENIX Collaboration 2004 *Phys. Rev. C* **69** 034909,
E866 Collaboration and E917 Collaboration 1999 *Phys. Lett. B* **476** 1,
NA44 Collaboration 1999 *Phys. Lett. B* **471** 6,
NA49 Collaboration 2002 *Phys. Rev. C* **66** 054902.
- [9] STAR Collaboration 2004 *Phys. Rev. Lett.* **93** 012301
- [10] Retiere F and Lisa M A 2004 *Phys. Rev. C* **70** 044907
- [11] STAR Collaboration 2005 *Phys. Rev. C* **71** 031901(R)
- [12] STAR Collaboration 2004 *Preprint* nucl-ex/0408012
- [13] STAR Collaboration 2004 *Preprint* nucl-ex/0411003
- [14] Kopytine M for the STAR Collaboration 2004 *Preprint* nucl-ex/0403011
- [15] STAR Collaboration 2004 *Preprint* nucl-ex/0406035
- [16] van Marcke E 1988 *Random Fields: Analysis and Synthesis* (Cambridge: The MIT Press)
- [17] Trainor T A, Porter R J and Prindle D J 2004 *Preprint* hep-ph/0410182
- [18] Flandrin P 1999 *Time-Frequency/Time-Scale Analysis* (San Diego: Academic Press) p.37
- [19] Liu Q, Trainor T A, and Prindle D J 2004 *Preprint* hep-ph/0410180